Structure and internal rotation of H_2O–CO_2, HDO–CO_2, and D_2O–CO_2 van der Waals complexes[a)]

K. I. Peterson and W. Klemperer
Department of Chemistry, Harvard University, Cambridge, Massachusetts 02138

(Received 21 October 1983; accepted 16 December 1983)

The radio frequency and microwave spectra of H_2O–CO_2, HDO–CO_2, and D_2O–CO_2 have been measured by molecular beam electric resonance spectroscopy. Rotational constants, deuterium quadrupole coupling constants, and dipole moments are reported.

	D_2O–CO_2	HDO–CO_2	H_2O–CO_2
$B + C$ (mHz)	7265.624(48)	7605.2(2)	7979.0(5)
$B - C$ (mHz)	1167.290(36)	1261.2(13)	1370.3(7)
$A - (B + C)/2$ (mHz)	7589.371(70)	7574(2)	7517(6)
$(eqQ)_a^D$ (kHz)	1(16)	−2(16)	...
$(eqQ)_b^O$ (kHz)	121(4)	127(16)	...
μ (0)	1.9285(10)	1.8911(10)	1.8515(10)

Analysis of the data shows the structure of the complex to be planar with C_{2v} symmetry with the hydrogens pointed away from the CO_2. A high barrier hindering the internal rotation of the H_2O with respect to the CO_2 around the a axis is observed; the height of the barrier is estimated to be 0.9 ± 0.2 kcal/mol.

I. INTRODUCTION

The interaction of water and carbon dioxide is a topic of importance in biochemical, atmospheric, laser, and industrial systems. For example, a considerable amount of research has been concerned with catalysis of the aqueous reaction of H_2O and CO_2 to form carbonic acid.[1] In a completely different area, the relaxation and excitation of vibrational states of CO_2 by H_2O have been studied and shown to be very fast and specific with respect to the particular vibrational state which is populated.[2] Many of the studies indicate some microscopic characteristics but direct experiments which probe the structure and bonding of water with CO_2 are necessary to further an understanding of the more complex systems. In this report we examine the weakly bound binary complex formed by these species.

There has been some previous work done on the CO_2–H_2O complex. Gas phase experiments involving the solubility of water in compressed CO_2 have resulted in a determination of second cross virial coefficients.[3] In the analysis, the occurrence of carbonic acid in the gas phase was suggested but Jönsson *et al.*[4] have disagreed with such a conclusion and claim that the results can be explained by van der Waals complexation of water with carbon dioxide. Using molecular orbital calculations, they predict a T-shaped, planar structure with the hydrogens directed away from the CO_2 and a C–O bond length of 2.63 Å. The van der Waals bond in this configuration was found to be 1.27 kcal/mol stronger than that with the hydrogens 90° out of the plane and 3.25 kcal/mol stronger than a hydrogen bonded structure. In agreement with this, a matrix isolation infrared spectroscopic study[5] has detected the presence of a T-shaped structure and no evidence of a hydrogen bonded structure was found.

Because of a general interest in interactions of CO_2 with other atoms and molecules, a number of different complexes have been studied.[6–8] Ar has been shown to act as a Lewis base in the T-shaped Ar–CO_2 complex. HF and HCl, on the other hand, are hydrogen bonded in a linear arrangement. Finally, HCN–CO_2 has recently been found to be T shaped with the nitrogen bound to the CO_2.[9] Using Lewis acid–base arguments, H_2O–CO_2 is also expected to be T shaped since H_2O is more basic than HCN.

II. EXPERIMENTAL

Transitions at radio and microwave frequencies were observed by means of a Rabi-type molecular beam electric resonance spectrometer with a mass spectrometer detector. This apparatus has been described in detail elsewhere.[10] The transition frequencies observed for these complexes ranged from 0.5 MHz to 17.5 GHz. The complexes are very asymmetrical tops with asymmetry parameters κ of about −0.7. The large number of easily observable asymmetry doublets in the radio-frequency region resulted in a quick and successful search for the first transition. Assignment of transitions found in this region was facilitated by use of the Stark effect. The location of transitions in the microwave region could then be predicted.

Production of H_2O–CO_2 complexes is straightforward. A mixture of argon gas containing 7% CO_2 and saturated

[a)]This work was supported by the National Science Foundation.

 0021-9606/84/062439-07$02.10

TABLE I. Observed zero field transitions of D_2O–CO_2.[a]

Assignment	Observed (MHz)	Obs.–Calc. (kHz)
1_{01}–0_{00}	7 265.550 (50)	11
2_{02}–1_{01}	14 396.900 (40)	– 5
2_{11}–1_{10}	15 695.560 (100)	10
1_{10}–1_{11}	1 166.360 (5)	– 0
2_{11}–2_{12}	3 498.780 (20)	– 0
2_{20}–2_{21}	133.662 (25)	– 6
3_{21}–3_{22}	657.000 (40)	16
3_{30}–3_{31}	9.627 (40)	5
4_{31}–4_{32}	66.856 (200)	– 4
4_{40}–4_{41}	0.578 (10)	7
5_{41}–5_{42}	5.114 (40)	– 5
6_{42}–6_{43}	25.362 (30)	– 28
3_{21}–4_{04}	3 842.240 (70)	– 2
3_{03}–2_{20}	9 346.252 (65)	3

[a] Uncertainties given are full width at half-maximum.

TABLE III. Observed zero field transitions of H_2O–CO_2.[a]

Assignment	Observed (MHz)	Obs.–Calc. (kHz)
1_{01}–0_{00}	7 978.562 (10)	– 0.3
2_{02}–1_{01}	15 771.229 (30)	– 104
2_{11}–1_{10}	17 326.398 (15)	283
1_{10}–1_{11}	1 369.455 (10)	359
3_{12}–3_{13}	8 198.843 (50)	– 1808
2_{20}–2_{21}	185.388 (2)	– 30
3_{30}–3_{31}	15.889 (3)	25
4_{31}–4_{32}	110.074 (15)	136
5_{32}–5_{33}	431.084 (15)	307
6_{33}–6_{34}	1 244.736 (3)	3
4_{40}–4_{41}	1.111 (3)	– 12
5_{41}–5_{42}	9.943 (2)	– 104
6_{42}–6_{43}	49.662 (5)	– 16

[a] Uncertainties given are full width at half-maximum.

with water was expanded through a 25 μ nozzle. The total pressure behind the nozzle was 2.5 atm. The fragment peaks at masses 45 (HCO_2^+) and 46 (DCO_2^+) are more intense than the parent peaks and were monitored in these experiments. More recently, the resonance signal of the 3_{13}–3_{12} transition of H_2O–CO_2 was measured at different mass peaks. The relative signal intensities for masses 18 (H_2O^+), 45 (HCO_2^+), 44 (CO_2^+), 28(CO^+), 17 (OH^+), 12 (C^-), 62 ($H_2OCO_2^+$), and 16 (O^+) are 20, 6.5, 6.5, 4, 3, 2, 0.2, and 0, respectively. In retrospect, monitoring the H_2O^+ peak would be a better choice in these experiments.

The observed zero field transitions of D_2O–CO_2, HDO–CO_2, and H_2O–CO_2 are given in Tables I, II, and III, respectively. The Hamiltonian derived by Watson[11] for a semirigid rotor was used to analyze the data:

$$H = [(B+C)/2]J^2 + [A-(B+C)/2]J_a^2 + [(B-C)/2](J_b^2 - J_c^2) - \Delta_J J^4 - \Delta_{JK} J^2 J_a^2 - \Delta_K J_a^4 - 2\delta_J J^2(J_b^2 - J_c^2) - \delta_K[J_a^2(J_b^2 - J_c^2) - (J_b^2 - J_c^2)J_a^2].$$

The large asymmetry of the complex allows $A - \Delta_K$ to be determined using just $\Delta K_{-1} = 0$ transitions and inclusion of $\Delta K_{-1} = 2$ transitions increases the accuracy of this determination. These latter transitions become more intense as κ approaches zero. In order to separately determine A and Δ_K, b- or c-type transitions are required. Since none of these were observed, no attempt was made to fit Δ_K and it was set equal to zero in the analysis. Its actual value is expected to be small enough that its removal would not substantially affect the value of $A - (B+C)/2$.

Using the above Hamiltonian, the D_2O–CO_2 spectrum can be reproduced very well and the fitted rotational and centrifugal distortion constants are given in Table IV. The fitting of the HDO–CO_2 and H_2O–CO_2 spectra were not successful as can be seen by comparing the observed-calculated frequencies given in Tables I, II, and III. While the residuals are within experimental error for D_2O–CO_2, they are greater for HDO–CO_2 and the worst fit occurs for H_2O–CO_2. In addition to difficulties with fitting the spectra, the resulting centrifugal distortion constants derived for HDO–CO_2 and H_2O–CO_2 were very unreasonable. These observations question the use of a semirigid rotor model and are indicative of the presence of hindered internal motion. The calculated energy level diagram for D_2O–CO_2 is shown in Fig. 1. Not included are effects of perturbations due to the hindered internal motion.

In a structural analysis, a set of rotational constants for at least two isotopes are necessary to determine the position of the water with respect to the CO_2 molecule. Since approxi-

TABLE II. Observed zero field transitions of HDO–CO_2.[a]

Assignment	Observed (MHz)	Obs.–Calc. (kHz)
1_{01}–0_{00}	7 605.216 (50)	– 3
2_{02}–1_{01}	15 053.745 (60)	4
2_{11}–1_{10}	16 468.214 (100)	– 10
1_{10}–1_{11}	1 260.321 (10)	– 1
2_{11}–2_{12}	3 780.600 (200)	63
3_{13}–3_{13}	7 547.858 (20)	275
2_{20}–2_{21}	156.080 (20)	– 15
3_{30}–3_{31}	12.193 (15)	3
4_{31}–4_{32}	84.609 (7)	2
5_{32}–5_{33}	332.578 (12)	– 220
4_{40}–4_{41}	0.782 (18)	– 6
5_{41}–5_{42}	6.990 (30)	– 65
6_{42}–6_{43}	34.675 (100)	– 271

[a] Uncertainties given are full width at half-maximum.

TABLE IV. Spectroscopic constants.[a]

	D_2O–CO_2	HDO–CO_2	H_2O–CO_2
$B+C$	7265.62 (48)	7605 (2)	797
$B-C$	1167.29 (36)	126	136
$A-(B+C/2)$	7589.37 (7)	75	75
Δ_J	0.021		
Δ_{JK}	0.30 (1)		
δ_J	0.006		
δ_K	0.22		
$(eqQ)_a^D$ (kHz)	1 (16)	– 2 (16)	
$(eqQ)_a^D$ (kHz)	121 (4)	127 (16)	
μ(D)	1.9291 (5)	1.8917 (5)	1.852 15 (20)

[a] Frequencies in MHz except where labeled. Errors in the brackets are two standard deviations.

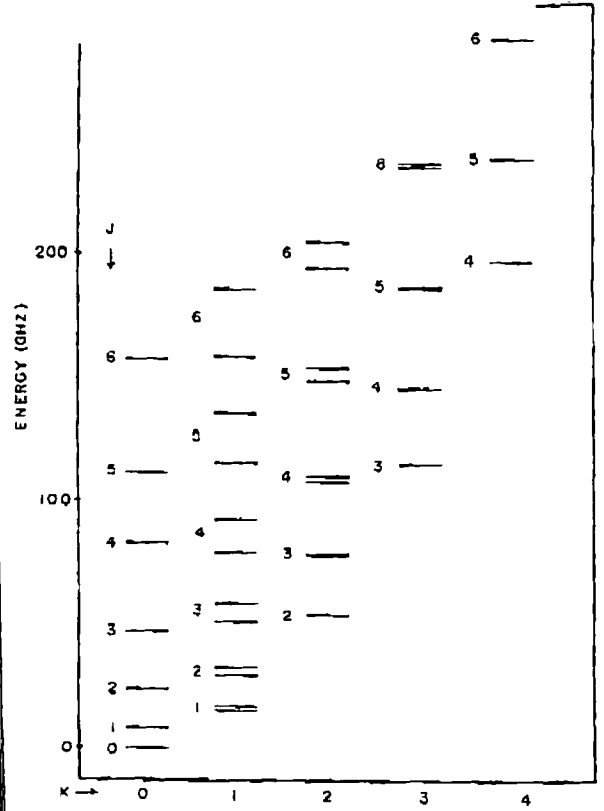

FIG. 1. Semirigid rotor energy level diagram of D_2O–CO_2 with rotational constants, $A = 11\,222$, $B = 4216$, and $C = 3049$ MHz. Actual levels will be shifted as described in the text and in Fig. 3.

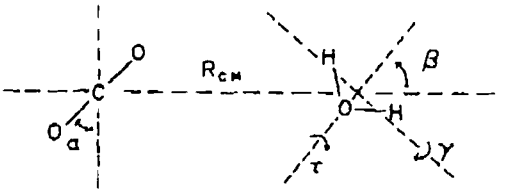

FIG. 2. Reference configuration of the H_2O–CO_2 complex.

mate values suffice, estimates were made of A, B, and C for HDO–CO_2 and H_2O–CO_2 by fitting only the rotational constants to the Watson Hamiltonian while setting the centrifugal distortion constants equal to those derived for D_2O–CO_2 (see Table IV). The errors obtained using this fitting procedure are less than 0.2%, therefore the rotational constants can be used with confidence in the structural analysis.

III. STRUCTURAL ANALYSIS

Assuming that the individual molecules do not undergo structural changes upon complexation, the structure of the complex can be described by one bond distance R and four angles. These are shown in Fig. 2; one angle α describes the CO_2 orientation and three angles β, γ, and τ describe the H_2O orientation. All four angles are referred to a planar, T-shaped configuration which was approximately deduced from the observed rotational constants. The ability of such a structure to reproduce the rotational constants can be seen when the distance between the carbon atom in CO_2 and the oxygen atom in H_2O, R_{c-o}, is optimized by fitting the structurally calculated $B + C$ to the 1_{01}–0_{00} transition while setting $\alpha = \beta = \gamma = \tau = 0$. The generated constants, $B - C$ and A, are within 10 and 200 MHz, respectively, of those determined by analysis of the data and no improvement occurs when other configurations are tested. Note that the distance R_{c-o} given in Table V is very similar for all three isotopes. If the same procedure is followed for a T-shaped structure with the hydrogens directed toward the CO_2, one finds large differences in R_{c-o} for each isotope, contrary to the expected behavior.

The rotational constants indicate that it is reasonable to use the planar, T-shaped configuration as a reference and subsequently determine the manner in which the complex oscillates around this structure. The presence of high energy barriers at this reference structure are of particular interest and can be detected in the ground vibrational state spectra. If there is a barrier at either $\alpha = 0, \beta = 0$, or $\gamma = 0$, two isomers exist which are mirror images of each other and the higher the barrier the lower the tunneling frequency between the two forms. Each of the two inversion states has a different hydrogen nuclear spin function associated with it so that when the barrier is low or nonexistent an observed $\Delta K_{-1} = 0$ transition will contain only one spin state while in the case of a high barrier, i.e., when the first excited state is populated at a beam temperature of 10 K, both spin states will be observed in any given transition. Analysis of the hyperfine structure can determine which spin states are present in each rotational level and therefore indicate whether there exists a high inversion barrier in the complex.

The motion around the C_2 axis described by τ is an internal rotation and this, together with the spin statistics of the oxygen nuclei in CO_2, causes half of the energy levels to disappear. This will be explained in more detail in the next section. The result is that even K_{-1} levels will contain one spin state and odd levels contain the other. If the barrier is low, the odd levels will be at a much higher energy relative to the even levels, but they still will be populated even in a cold molecular beam because there is no mechanism for relaxation to a level of a different spin state.

Thus, observation of only one spin state in a rotational transition implies that there is a low or nonexistent barrier at $\alpha = 0, \beta = 0$, and $\gamma = 0$. This is indeed what is observed and the data will be presented in the next section. This information is not sufficient for differentiating between a low and high barrier for the internal rotation but since the spectra indicate that a hindered internal motion is present we are only left with the latter possibility.

In the next three sections, data will be presented which are consistent with a planar, C_{2v}, equilibrium structure. In addition to an analysis of the molecular symmetry, an analysis is made of the hyperfine structure in HDO–CO_2 and

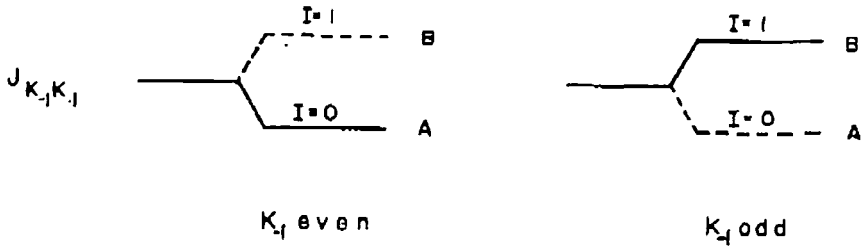

FIG. 3. The effect of internal rotation on the rotational energy levels. The spin statistics of the identical hydrogen and oxygen nuclei cause half of the levels to disappear (dotted lines) and the spin state of the odd and even levels to be different. The nuclear spin labels refer to the hydrogen nuclei, the total spin of which is 1.

D_2O–CO_2 which shows that the vibrationally averaged value for the angle τ is relatively small implying that the barrier to the internal rotation is at $\tau = 90°$ rather than 0°. Finally, dipole moment comparisons of the three isotopes give further evidence for very low inversion barriers.

A. Symmetry considerations

For a T-shaped, internally rotating complex, H_2O–CO_2 and D_2O–CO_2 have two pairs of equivalent nuclei and HDO–CO_2 has one. This equivalence can be observed by measuring the hyperfine structure of an odd and even K_{-1} level. Each level is split by an internal rotation around the C–O bond into a symmetric and antisymmetric state, the former having the lowest energy. Since the oxygen nuclei are spin zero particles and therefore follow Bose–Einstein statistics, the total wave function must be symmetric upon interchange of oxygen nuclei. This requirement allows only those levels to exist whose rotational and torsional states have the same symmetry. This condition is pictured in Fig. 3.

In H_2O–CO_2, the hydrogen nuclei each have a spin of 1/2 so that the total spin state will be symmetric ($I = 1$) or antisymmetric ($I = 0$). Since Fermi–Dirac statistics apply, the total wave function must be antisymmetric with respect to interchange of hydrogen nuclei. For this to occur, only antisymmetric spin states exist when K_{-1} is even and symmetric states exist when K_{-1} is odd. Therefore even K_{-1} levels will exhibit a singlet and odd levels will exhibit a triplet hyperfine pattern. The deuterium nuclei in D_2O–CO_2 follow Bose–Einstein statistics and the reverse argument is made. The spin state is symmetric ($I = 0, 2$) when K_{-1} is even and antisymmetric ($I = 1$) when it is odd.

The hyperfine structure is simpler in H_2O–CO_2 and the singlet and triplet states can be observed in the even and odd levels, respectively, thereby showing that the hydrogen nuclei are identical. The lack of hyperfine structure in the 2_{20}–2_{21} transition in Fig. 4 is consistent with a singlet spin state. In Fig. 5, a calculated hydrogen spin–spin hyperfine pattern for the triplet ($I = 1$) state is shown which reproduces the observed structure in the 1_{10}–1_{11} transition. Since this spectrum could only be partially resolved, the projection of the spin–spin hyperfine tensor on the a, b, and c axes could not be determined accurately.

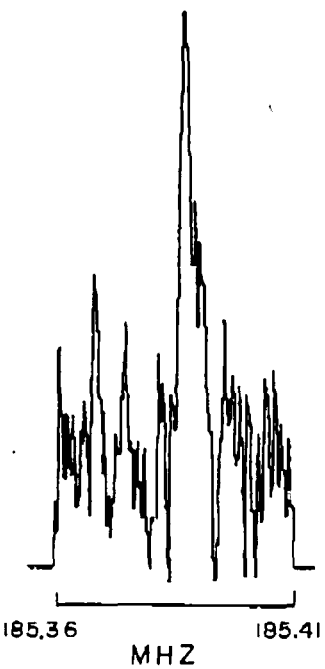

FIG. 4. The 2_{20}–2_{21} transition of H_2O–CO_2. No hyperfine structure is observed.

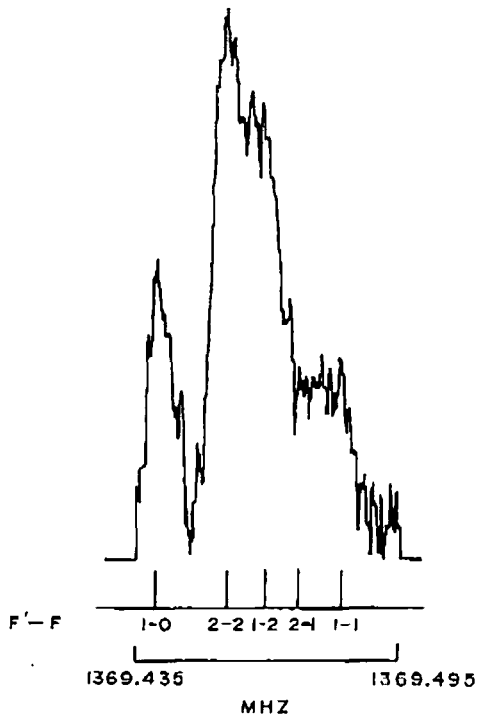

FIG. 5. The 1_{10}–1_{11} transition of H_2O–CO_2. Included below the observed spectrum is a stick spectrum calculated using $\langle P_2(\cos\theta_a)\rangle = 0.81$ and $\langle P_2(\cos\theta_b)\rangle = -0.37$.

B. Hyperfine spectrum

The hyperfine splitting in the $K_{-1} = 1$ asymmetry doublet is observable in HDO–CO_2 and D_2O–CO_2 and from it the quadrupole coupling constant is obtained. The hyperfine Hamiltonian used for HDO–CO_2 is

$$H_{hfs} = \frac{2}{J(J+1)}\left[\sum_g (eqQ)_g^p \langle J_g^2 \rangle\right] Y(J, I, F).$$

$Y(J, I, F)$ is Casimir's function and the $(eqQ)_g^p$ are the quadrupole coupling constants along the inertial axes. The contribution due to spin rotation is less than 1 kHz and has not been included. The H–D spin–spin interaction is also small and is the cause of the 10 kHz linewidth of each hyperfine component.

The hyperfine Hamiltonian for D_2O–CO_2 is

$$H_{hfs} = H_{Q_1} + H_{Q_2}.$$

The matrix elements for two identical nuclei are best evaluated in a $(I_1 I_2 JJFM_F)$ representation.[13,14] Both the spin-rotation and spin–spin interactions are neglected. As mentioned previously, the $K_{-1} = 1$ levels are simplified by the absence of $I = 0$ and $I = 2$ spin states. An effective spin quantum number of 1 produces a spectrum which is similar to that of HDO–CO_2.

Analysis of the hyperfine structure results in values for the quadrupole coupling constants along the a and b axes using the fact that the trace of the quadrupole tensor is zero. From these, the average projection of the OD bond on each axis is obtained using the equation

$$(eqQ)_g^p = (eqQ)_c^p \langle P_2(\cos \vartheta_g) \rangle.$$

$(eqQ)_c^p$, the quadrupole coupling constant along the OD bond, was determined by Thaddeus *et al.*[12] to be 318.6 kHz in the 2_{20}–2_{21} transition of HDO. ϑ_g is the angle which the O–D bond makes with the g axis.

The measured hyperfine transitions for HDO–CO_2 and D_2O–CO_2 are listed in Table VI and the derived quadrupole coupling constants are given in Table IV. The resulting projection angles given in Table V are very close to the equilibrium angles expected for a planar, C_{2v} structure, i.e., $\vartheta_a = 52.25°$ and $\vartheta_b = 37.75°$.

Two angles were determined by the above analysis but four angles are needed to describe the complex. The angle α can be separated from the other three angles for purposes of hyperfine analysis since α has no effect on the values of the projections of the quadrupole coupling constant. Later, when the rotational constant A is corrected for internal rotation effects, an estimate can be made for α. Changes in β do affect the splitting but this effect is smaller than that produced by changes in either γ or τ. This arises from the fact that the equilibrium angle is 52.25° rather than 0°. The closer the angle is to 45°, the more similar the average angle is to the equilibrium angle. By expanding the average projection $\langle P_2(\cos \vartheta) \rangle$ around an equilibrium values of 52.25° one finds that the average deviation is about one fourth of that found when the equilibrium angle is 0°. The contribution of β to $\langle P_2(\cos \vartheta) \rangle$ is therefore not negligible but will be omitted in order to obtain an estimate for τ and γ. In fact, the values obtained will be upper and lower limits, respectively, to the actual average values.

τ and γ are related to ϑ_a and ϑ_b by the following:

$$\cos \gamma = \cos \vartheta_a / \cos \beta_c,$$
$$\cos \tau = \cos \vartheta_b / \sin \beta_c.$$

Therefore, for D_2O–CO_2, one obtains $\gamma = 19°$ and $\tau = 15°$. Both of these are consistent with the large amplitude motions typical for weakly bound complexes.

TABLE V. Derived structural parameters.

	D_2O–CO_2	HDO–CO_2	H_2O–CO_2
$R_{c.m.}$ (Å)	2.821	2.826	2.836
θ_a (deg)	54.6 (20)	55.0 (20)	...
ϑ_b (deg)	40.0 (5)	39.3 (20)	...

TABLE VI. Hyperfine spectrum of the 1_{10}–1_{11} transition (in mHz).

F–F'	Observed	Calculated
D_2O–CO_2		
1 0	1166.329 (3)	1166.329
2 2	1166.347 (3)	1166.347
2 1	1166.384 (3)	1166.3842
1 2		1166.3839
1 1	1166.420 (2)	1166.420
	Center frequency 1166.360	
HDO–CO_2		
2 1	1260.296 (10)	
2 2	1260.334 (10)	
0 1	1260.352 (10)	
	Center frequency 1260.321	

C. Dipole moment measurements

The dipole moment for each isotope was determined by measuring the effect of an electric field on the $M_J = 0$–1 transition in the 1_{01} level. Matrix elements of the electric field perturbed Hamiltonian were calculated in the basis $|JKM_J\rangle$ including $J = 0$ to $J = 3$ levels. The deuterium hyperfine splitting in these transitions is small and is therefore ignored in the calculation. Observed and calculated transitions are listed in Table VII and the resulting dipole moments can be found in Table IV. The larger error in the HDO–CO_2 and D_2O–CO_2 measurements reflects the presence of unresolvable hyperfine structure.

Since the dipole moments of H_2O and D_2O are essentially the same (1.8546 and 1.8545 D, respectively[15,16]), the differences in the complexes reflect the amplitudes of the zero point oscillations. The oscillations which involve the hydrogen atoms have larger amplitudes in H_2O–CO_2, coincidental with a lower average dipole moment. The fact that the dipole moment increases substantially upon deuteration once again points to a planar geometry as the equilibrium structure. Using the lower limit of γ found in the previous section along with the dipole moment for D_2O, the contribution of D_2O to the total dipole moment is 1.7535 D along the a axis. Since CO_2 is nonpolar the lower limit for the induced dipole moment is 0.175 D.

TABLE VII. $M_J = 0$–1 transitions in the $J = 1$, $K_{-1} = 0$ level at various stark fields (in MHz).

	H_2O–CO_2		HDO–CO_2		D_2O–CO_2	
Voltage[a]	Obs.	Calc.	Obs.	Calc.	Obs.	Calc.
500.21 (1)	7.909 (3)	7.909	8.656 (10)	8.655	9.421 (10)	9.420
700.40 (1)	15.492 (5)	15.492	16.949 (15)	16.951	18.446 (15)	18.448
800.37 (1)	20.218 (2)	20.218	22.120 (20)	22.121	24.064 (20)	24.072
900.33 (1)	25.568 (3)	25.567	27.976 (20)	27.971	30.438 (20)	30.435

[a] Voltage (in V) applied between 1.016 cm separated plates.

D. Internal rotation

In summary, the good fit of the D_2O–CO_2 spectrum compared to that of HDO–CO_2 and H_2O–CO_2 indicates the presence of a fairly high barrier to an internal motion. The rotational constants, hyperfine spectra, and dipole moments all point to a planar C_{2v} structure and therefore high barriers hindering the inversion motions at the T-shaped, planar configuration are not possible. The only van der Waals vibrational motion which can experience a high barrier is the rotation of the two molecules with respect to each other around the a axis.

A complete and quite readable theoretical treatment of hindered rotation with a twofold potential barrier was derived by Quade.[17] In this treatment the molecule is assumed to be rigid except for one degree of freedom for the internal rotation. The potential energy as a function of this degree of freedom is taken as

$$V(\tau) = \tfrac{1}{2}V_2(1 - \cos 2\tau).$$

The result of the derivation for the special case when both parts of the molecule possess twofold axes of symmetry is the effective Hamiltonian

$$H_{n\sigma} = \tfrac{1}{2}(B_{n\sigma} + C_{n\sigma})(P_y^2 + P_x^2) + A_{n\sigma}P_z^2 + \tfrac{1}{2}(B_{n\sigma} - C_{n\sigma})(P_y^2 - P_x^2) + E_{n\sigma}.$$

The parameters n and σ label the torsional states and substates, respectively. In the problem presented here, we will only be concerned with the two substates of the ground torsional state.

The derived rotational constants include rigid rotor terms along with first, second, and third order corrections. Since the moment of inertia of D_2O or H_2O around the principal axis is much smaller than that of the entire molecule, many of the correction terms are small enough to be neglected. The resulting truncated forms of the corrected rotational constants are

$$B_{n\sigma} + C_{n\sigma} = \mu_{yy}^0 + \mu_{xx}^0 + (\mu_{yy}^{(2)} + \mu_{xx}^{(2)})\langle n\sigma|\sin^2\alpha|n\sigma\rangle_1,$$

$$B_{n\sigma} - C_{n\sigma} = \mu_{yy}^0 - \mu_{xx}^0 + (\mu_{yy}^{(2)} - \mu_{xx}^{(2)})\langle n\sigma|\sin^2\alpha|n\sigma\rangle_1,$$

$$A_{n\sigma} = \mu_{zz}^0 + 4[(\mu_{zz}^0)^2/\mu_T^0]\,\langle n\sigma|P^2|n\sigma\rangle_2.$$

μ_{ii}^0, $\mu_{ii}^{(2)}$, and μ_T^0 are moment of inertia terms and are defined in Quade's paper.[17] The matrix elements have been calculated by Herschbach[18] as a function of the parameter $s = V_2/\mu_T^0$.

In water–CO_2, different effective rotational constants apply for each set of levels (σ_A and σ_B). By estimating the difference in the observed rotational constants for the upper and lower states and equating this to the difference between the correction terms in the above constants, an estimate can be made of V_2. Calculated values are required for

$$\Delta_1 \equiv \langle 0\sigma_A|\sin^2\alpha|0\sigma_A\rangle_1 - \langle 0\sigma_B|\sin^2\alpha|0\sigma_B\rangle_1$$

and

$$\Delta_2 \equiv \langle 0\sigma_A|P^2|0\sigma_A\rangle_2 - \langle 0\sigma_B|P^2|0\sigma_B\rangle_2$$

as a function of s. A sample of these, calculated from Herschbach's tables, are given in Table VIII.

D_2O–CO_2 is more amenable to analysis since the distortion terms are accurately determined. For this complex, the values of the rotational constants $B + C$ and $B - C$ are the same for the even (σ_A) and odd (σ_B) K_{-1} levels fitted separately. Therefore the uncertainties in the constants as given in Table IV can be used as an upper limit for $\Delta(B + C)$ and $\Delta(B - C)$ which in turn will give a lower limit for V_2 of 0.7 kcal/mol. The A rotational constant is different for the odd and even levels with $\Delta A = 600$ kHz and from this $V_2 = 1.1$ kcal/mol is determined to be 1.1 kcal/mol. When this value of V_2 is used to calculate ΔA, $\Delta(B + C)$, and $\Delta(B - C)$ for H_2O–CO_2, values are obtained which are considerably smaller than the uncertainties given in Table IV so 1.1 kcal/mol is taken as an upper limit for the barrier height. A complete treatment of this one-dimensional model was not attempted since it is unlikely to produce a more accurate value for the potential. The main problem concerns the fact that van der Waals complexes have other low frequency vibrations whose coupling with the internal rotation is unknown.

The resulting barrier, 0.9 ± 0.2 kcal/mol, is smaller than that calculated by Jönsson *et al.*,[4] 1.3 kcal/mol, but is still considered high compared to the van der Waals bond

TABLE VIII. Calculated matrix elements for internal rotation problem.

s[a]	Δ_1[a]	Δ_2[a]
10	3.6×10^{-2}	1.52×10^{-1}
20	3.5×10^{-3}	2.06×10^{-2}
28	7.7×10^{-4}	5.26×10^{-3}
36	2.0×10^{-4}	1.57×10^{-3}
40	1.1×10^{-4}	8.90×10^{-4}
48	4.0×10^{-5}	3.07×10^{-4}
56	1.0×10^{-5}	1.15×10^{-4}

[a] $S = V_2/\mu_T^0$, $\Delta_1 = \langle 0\sigma_A|\sin^2\alpha|0\sigma_A\rangle_1 - \langle 0\sigma_B|\sin^2\alpha|0\sigma_B\rangle_1$, $\Delta_2 = \langle 0\sigma_A|P^2|0\sigma_A\rangle_2 - \langle 0\sigma_B|P^2|0\sigma_B\rangle_2$.

strength of about 6 kcal/mol. From the experimentally determined barrier, the effective energy level splitting ΔE for the rotational levels can be estimated. For D_2O–CO_2, $\Delta E = 75$ MHz while for H_2O–CO_2, $\Delta E = 3500$ MHz. As has been discussed, half the levels do not exist and therefore this splitting is present as a shift between odd and even K_{-1} levels. Direct transitions between different torsional states ($\Delta K_{-1} = 1, 3, \ldots$) are forbidden for the symmetric species H_2O–CO_2 and D_2O–CO_2 but are allowed for HDO–CO_2 since it has a small dipole moment along the b or c axis. Such transitions were not observed in these experiments.

We should note here that the values of the internal rotation correction terms which must be added to the semirigid rotor rotational constants to obtain the observed constants can be quite large even though their difference for the two torsional states is very small. The A rotational constant in particular has a large correction term connected with it since the internal rotation coupling is strongest with P_z. For D_2O–CO_2, estimates of the correction terms for $B + C$, $B - C$, and A are 0.4, 1.4, and 880 MHz, respectively.

Estimates of the semirigid rotor rotational constants are obtained by adding the correction terms to the measured constants. Using the corrected value of A (12 100 MHz) the structural parameter α can now be estimated since A is a strong function of this parameter. Structural analysis results in a value of α of 17°. This value is higher than other van der Waals complexes; for example, the CO_2 bending angle in HCN–CO_2 is 11°.[9] This discrepancy probably reflects the large error in the correction term. Neglecting higher order correction terms as was done in this analysis has a larger effect on the absolute values of the rotational constants than on their difference.

IV. DISCUSSION

The present structural and dynamical results are in qualitatively good agreement with the self-consistent field calculations of Jönsson, Karlström, and Wennerström.[4] In view of the general importance of the H_2O–CO_2 system it would be highly desirable to have more complete electron structure calculations for the system. The present interpretation of the spectral data obtains an estimate for the barrier hindering internal rotation ignoring other vibrations. Clearly, a more complete potential energy surface could be of value in providing a model useful for understanding this and other dynamical characteristics. Further experimental work particularly on b-type transitions of HDO–CO_2 will provide a more quantitative estimate for the hindered rotations.

There are a number of remarks to be made on this system. This work confirms the infrared spectroscopic study of Fredin, Nelander, and Ribbegard[5] that suggests that the structure is not hydrogen bonded. The planar, quite rigid structure is qualitatively understandable in terms of the interaction of the H_2O lone pairs with the CO_2 $2\pi_u$ unoccupied orbital. In this sense, the complex would be characterized by π type bonding. We note that H_2O–CO_2 is isoelectronic to H_2CCF_2 in which the origin of planar rigidity is clearly the π bond. H_2NNO_2, also isoelectronic, has been studied by Tyler[19] and found to be nonplanar although less so than NH_3. The barrier to internal rotation was not estimated for this species. In this case, our simplistic view that isoelectronic systems are frequently structurally isomorphic is not accurate.

We conclude by noting that the binding complex H_2O–CO_2 is only partially similar to the chemical view of carbonic acid.[20] Since the reaction of H_2O and CO_2 in the aqueous phase is catalyzed by H_2O,[1] the complex $(H_2O)_2CO_2$ would more likely show both the CO_3 moiety and incipient OH pairs of chemical H_2CO_3. In view of the likely complexity in the rotation spectrum of this species, it would be quite useful to have good theoretical estimates of conceivable structural and dynamical complexities which may be encountered.

[1] Y. Pocker and D. W. Bjorkquist, J. Am. Chem. Soc. 99, 6537 (1977).
[2] (a) J. A. L. Lewis and K. P. Lee, J. Acoust. Soc. Am. 38, 813 (1965); (b) F. D. Shields and J. A. Burks, *ibid.* 43, 510 (1968).
[3] C. R. Coon and A. D. King, Jr., J. Am. Chem. Soc. 93, 1857 (1971).
[4] B. Jönsson, G. Karlström, and H. Wennerström, Chem. Phys. Lett. 30, 58 (1975).
[5] L. Fredin, B. Nelander, and G. Ribbegård, Chem. Scr. 7, 11 (1975).
[6] F. A. Baiocchi, T. A. Dixon, C. H. Joyner, and W. Klemperer, J. Chem. Phys. 74, 6544 (1981).
[7] R. S. Altman, M. D. Marshall, and W. Klemperer, J. Chem. Phys. 77, 4344 (1982).
[8] J. M. Steed, T. A. Dixon, and W. Klemperer, J. Chem. Phys. 70, 4095 (1979).
[9] K. L. Leopold, G. T. Fraser, and W. Klemperer, J. Chem. Phys. 80, 1039 (1984).
[10] T. R. Dyke, G. R. Tomasevich, and W. Klemperer, J. Chem. Phys. 57, 2277 (1972).
[11] J. K. G. Watson, J. Chem. Phys. 46, 1935 (1967).
[12] P. Thaddeus, L. C. Krisher, and S. H. N. Loubser, J. Chem. Phys. 40, 257 (1964).
[13] R. L. Cook and F. C. DeLucia, Am. J. Phys. 39, 1433 (1971).
[14] F. C. DeLucia and J. W. Cederberg, J. Mol. Spectrosc. 40, 52 (1971).
[15] S. A. Clough, Y. Beers, G. P. Klein, and L. S. Rothman, J. Chem. Phys. 59, 2254 (1973).
[16] T. R. Dyke and J. S. Muenter, J. Chem. Phys. 59, 3125 (1973).
[17] C. R. Quade, J. Chem. Phys. 47, 1073 (1967).
[18] D. R. Herschbach, Tables for the Internal Rotation Problem, Harvard University, Massachusetts.
[19] J. K. Tyler, J. Mol. Spectrosc. 11, 39 (1963).
[20] B. Jönsson, G. Karlström, and H. Wennerström, Chem. Phys. Lett. 41, 317 (1976).